ACS Catalysis

pubs.acs.org/acscatalysis

Research Article

Mechanistic Insights into the Lanthanide-Catalyzed Oxychlorination of Methane as Revealed by *Operando* Spectroscopy

Bas Terlingen, Ramon Oord, Mathieu Ahr, Eline Hutter, Coert van Lare, and Bert M. Weckhuysen*

Cite This: *ACS Catal.* 2021, 11, 10574–10588

Read Online

ACCESS | Metrics & More | Article Recommendations | Supporting Information

ABSTRACT: Commercialization of CH_4 valorization processes is currently hampered by the lack of suitable catalysts, which should be active, selective, and stable. CH_4 oxychlorination is one of the promising routes to directly functionalize CH_4, and lanthanide-based catalysts show great potential for this reaction, although relatively little is known about their functioning. In this work, a set of lanthanide oxychlorides (*i.e.,* LnOCl with Ln = La, Pr, Nd, Sm, Eu, Gd, Tb, Dy, and Ho) and Er- and Yb-based catalysts were synthesized, characterized, and tested. All lanthanide-based catalysts can directly activate CH_4 into chloromethanes, but their catalytic properties differ significantly. EuOCl shows the most promising catalytic activity and selectivity, as very high conversion levels (>30%) and chloromethane selectivity values (>50%) can be reached at moderate reaction temperatures (~425 °C). *Operando* Raman spectroscopy revealed that the chlorination of the EuOCl catalyst surface is rate-limiting; hence, increasing the HCl concentration improves the catalytic performance. The CO selectivity could be suppressed from 30 to 15%, while the CH_4 conversion more than doubled from 11 to 24%, solely by increasing the HCl concentration from 10 to 60% at 450 °C. Even though more catalysts reported in this study and in the literature show a negative correlation between the S_{CO} and HCl concentration, this effect was never as substantial as observed for EuOCl. EuOCl has promising properties to bring the oxychlorination one step closer to an economically viable CH_4 valorization process.

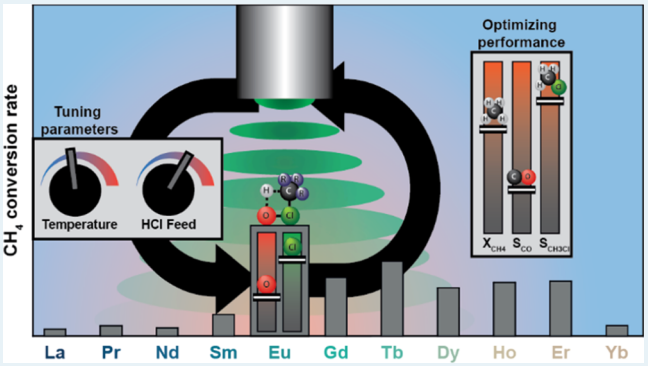

KEYWORDS: *lanthanide, methane, oxychlorination, reaction mechanism, operando spectroscopy*

1. INTRODUCTION

The use of CH_4 from natural gas in chemical industry is expected to grow in the coming years, especially in view of the lower CO_2 footprint relative to other fossil-based resources, such as coal and crude oil.[1] CH_4 is used in the synthesis of chemical building blocks, such as ammonia, methanol, and acetic acid.[2,3] Central in the synthesis of these molecules is the partial oxidation of methane to CO and H_2 *via* reforming reactions, followed by one or more synthesis steps to obtain the desired reaction product.[4] A major drawback of this approach is the energy-intensive, multistep process to obtain the desired bulk chemicals. Direct conversion routes of CH_4 into chemical building blocks could reduce the energy needed for CH_4 upgrading. To this date, however, direct conversion routes have not been commercialized because high selectivity is often only achieved at low conversion levels, while high conversion levels lead to the formation of, for example, CO_2.[2,5]

The direct conversion of CH_4 into halogenated CH_4, such as CH_3Cl and CH_3Br, *via*, for example, methane oxychlorination (MOC)[6−11] and methane oxybromination,[8,12−15] is a promising route for efficient hydrocarbon utilization.[16] Compared to other direct conversion routes of CH_4, high selectivity to the desired product and relatively high conversions can be achieved, while being operated under moderate reaction conditions (*i.e.,* in the 400−600 °C temperature range and with p = ~1 bar).[14] Chlorinated methanes (CMs) are commodity chemicals, and CH_3Cl is especially of great interest due to the chemical analogy between CH_3Cl and CH_3OH.[9,17] It can serve as a building block for the production of added value commodity chemicals, such as ethylene, propylene, and acetic acid.[5,18] Therefore, a high selectivity to the desired CH_3Cl is of great interest in the open literature[8−11,14,19−22] and in the patent literature.[18,23−28] However, the selective conversion of CH_4 into CH_3Cl remains challenging. The polarized bonds in the functionalized molecule are often more reactive than the inert C−H bonds present in CH_4, resulting in undesired byproduct formation.[2,5] For MOC, other chlorinated products, such as CH_2Cl_2, are thus also obtained. In the upgrading of CH_3Cl into olefins, even small amounts of CH_2Cl_2 cause rapid zeolite deactivation and thus

Received: January 27, 2021
Revised: July 17, 2021
Published: August 10, 2021

https://doi.org/10.1021/acscatal.1c00393
ACS Catal. 2021, 11, 10574−10588

CH_2Cl_2 needs to be removed from the feedstock.[20] This increases the cost to separate CH_3Cl and requires the development of, for instance, the hydrodechlorination process to convert poly-chlorinated CH_4 into CH_3Cl.[29]

Olah *et al.* found that inserting an electrophilic Cl atom catalytically over solid (super)acids could reverse CH_4 over-functionalization and obtain high yields toward CH_3Cl for direct chlorination.[30] However, the chlorination of CH_4 *via* the oxychlorination reaction is preferred because it utilizes HCl, produced as a byproduct in chlorination reactions, with a 100% Cl atom efficiency. In comparison, the Cl atom efficiency of thermal chlorination reactions is only 50%.[30] This concept of an electrophilic Cl atom was successfully adapted by Podkolzin, Lercher, and co-workers and applied in the MOC reaction over LaOCl.[10] Interestingly, a reaction mechanism was proposed where La^{3+} catalyzes the reaction without changing the oxidation state.[22] The activation of terminal surface lattice Cl by the dissociative adsorption of O_2 results in a surface hypochlorite (ClO^-), where the formal oxidation state of chlorine changes from −1 to +1. CH_4 coordinates to this hypochlorite, and an atom exchange occurs, leaving a hydroxyl group on the surface and the CM. This surface hydroxyl group reacts with HCl to regenerate the chlorinated surface, producing water. Bulk LaOCl catalysts with a S_{BET} of around 20 m^2/g were activated with HCl and were able to chlorinate CH_4.[10] At moderate conversion levels (X_{CH_4} = 10%), S_{CH_3Cl} ∼80% was obtained with minor byproducts of CH_2Cl_2 (12%) and CO (8%), essentially free of CO_2, $CHCl_3$, and CCl_4.[31]

However, the high selectivity was only obtained at low conversion levels (X_{CH_4} = <10%). As the conversion of CH_4 was increased (X_{CH_4} = ∼18%), the CO yield would surpass the CH_3Cl yield.[11] Overoxidation of CH_4 into CO_x at high conversion levels is the biggest challenge in the catalyst and process development for the MOC reaction.[8,32] Controlling the degree of surface chlorination of the solid catalysts, while maintaining a high conversion level is crucial for an economically viable process. For lanthanum-based catalysts, it is known that the CH_4 chlorination step leaves a terminal surface lattice oxygen, while the exact same site is also responsible for the catalytic destruction of polychlorinated hydrocarbons.[33] Balancing the chlorination rate with HCl and dechlorination rate by the reaction with CH_4 and O_2 is crucial for controlling the catalyst selectivity.

While a handful of publications report on the use of lanthanum,[10,11,21,22] cerium,[7,9,19] and europium[6] oxychlorides, the rest of the lanthanide series remains so far largely unexplored. Lanthanides are interesting due to their high stability in corrosive environments and tunable redox properties and are thought to exhibit comparable chemistry in the oxychlorination reaction.[18] Europium-based catalysts were previously reported as promising ethylene/propylene oxychlorination and CH_4 oxybromination catalysts.[6,13] The well-tailored redox properties of EuOX (with X = Cl or Br) were crucial in developing an active and selective catalysts.[6] Less successful was the use of EuOCl in MOC, where overoxidation seemed to be a large issue. For example, a S_{CO} value of ∼20% was observed at similar CH_4 conversion levels, which is too high for industrial application.[6]

In this work, we have performed a comprehensive study on the CH_4 oxychlorination over a series of lanthanide-based catalysts with the general formula LnOCl, where Ln = La, Pr, Nd, Sm, Eu, Gd, Tb, Dy, and Ho. Two other lanthanide catalysts, Er- and Yb-based, were also synthesized with the same synthesis technique, which did not yield the LnOCl phase. Although not all lanthanide-based catalysts showed equally high activity, this study revealed that they can be used to directly activate CH_4 into CMs. Moreover, we show that a EuOCl catalyst possesses unique characteristics that make it possible to develop catalysts with high conversions and low selectivity toward CO_x as unwanted byproducts. Central in this study is the possibility to operate a EuOCl catalyst in HCl-rich environments. The CO selectivity could be suppressed, while the CH_4 conversion more than doubled, solely by increasing the HCl concentration. Even though more reported catalysts show this behavior (*e.g.*, CeO_2 when HCl% 6% → 15%, X_{CH_4} ∼31% → ∼34% and S_{CO} ∼17% → ∼15%),[14] this effect was never as substantial as observed for EuOCl. Furthermore, new mechanistic insights into the working principles of this superior EuOCl catalyst material were obtained by using *operando* spectroscopy.

2. EXPERIMENTAL METHODS

2.1. Catalyst Synthesis. LnOCl (where Ln = La, Pr, Nd, Sm, Eu, Gd, Tb, Dy, and Ho) and Er- and Yb-based catalyst materials under study were prepared by dissolving the corresponding lanthanide(III) chloride salt ($LnCl_3{\cdot}xH_2O$, Fisher Scientific, >99%) in ethanol (absolute, VWR), followed by a precipitation using stoichiometric amounts of ammonium hydroxide (Fisher Scientific, 25% in H_2O) at room temperature. After the dropwise addition, the precipitates were stirred for an additional hour and subsequently centrifuged to obtain the gel. Then, the obtained gel was washed with ethanol (absolute, VWR) and dried at 80 °C. Lastly, the dried solids were calcined in a static oven at 500 °C for 3 h using a ramp rate of 5 °C/min.

2.2. Catalyst Characterization. X-ray diffraction (XRD) patterns were obtained with a Bruker-AXS D2 Phaser powder X-ray diffractometer in Bragg−Brentano geometry, using Co $K\alpha_{1,2}$ = 1.79026 Å, operated at 30 kV. The measurements were carried out between 10 and 80° using a step size of 0.05° and a scan speed of 1 s, with a 2 mm slit for the source. N_2 adsorption isotherms were measured at 77 K on a Micromeritics TriStar II Plus instrument. Prior to all measurements, samples were dried at 573 K under a flow of N_2. Specific surface areas were calculated using the multipoint BET method ($0.05 < p/p_0 < 0.25$). Pore volumes were calculated by the *t*-plot method; pore size distributions were obtained by BJH analysis. Transmission electron microscopy (TEM) was performed on a FEI Tecnai 20 instrument operating at 200 kV.

Operando spectroscopy measurements were performed with an AvaRaman-532 HERO-EVO instrument (λ = 532 nm, laser output 50 mW, spectral resolution of 10 cm^{-1}) equipped with an AvaRaman-PRB−FC−532 probe, capable of withstanding temperatures up to 500 °C. Spectra were collected every minute with the AvaSoft 8 software. The data were subsequently baseline corrected and normalized. The initial Raman intensity was optimized to obtain at least 50% of the saturation value. The *operando* Raman experiments were performed by a sequential chlorination, dechlorination and oxychlorination step. The chlorination reaction was performed at 450 °C with a HCl/N_2 ratio of 20:20 (mL/min) for 2 h. Subsequently, the reactor was heated to 500 °C under N_2, and then, flows $CH_4/HCl/O_2/N_2$/He of 2:0:1:1:16 and $CH_4/HCl/O_2/N_2$/He of 2:2:1:1:14 were applied for dechlorination (90 min) and oxychlorination (2 h), respectively. The *operando* photoluminescence spectroscopy

https://doi.org/10.1021/acscatal.1c00393
ACS Catal. 2021, 11, 10574−10588

experiments were performed by two sequential ramp experiments from 450 to 520 °C at 1 °C/min under the CH_4/HCl/O_2/N_2/He ratio of 2:2:1:1:14. Prior to the first ramp experiment, the catalyst was subjected to the ratio CH_4/HCl/O_2/N_2/He of 2:2:1:1:14 for 2 h at 450 °C. Prior to the second ramp experiment, the catalyst was subjected to a CH_4/HCl/O_2/N_2/He ratio of 0:4:0:1:14.

2.3. Catalyst Testing. All the catalytic tests and *operando* Raman measurements were performed in a lab-scale continuous-flow fixed-bed quartz reactor. Details of the setup, including a schematic and some pictures, are shown in Figure S1.

In a typical experiment, 500 mg of the catalyst material (with a 125−425 μm size fraction) was loaded in a quartz reactor and heated to 450 °C under N_2 with 10 °C/min. The catalyst was activated in 20% HCl/N_2 for 2 h prior to catalysis. For the isothermal experiments, the temperature was adjusted to reach X_{CH_4} = 10% for the CH_4/HCl/O_2/N_2/He ratio of 2:2:1:1:14. When stable conversion was reached, the HCl/He ratio was adjusted, so that the HCl concentration was increased to 20, 40, 60, and 80%, while keeping a constant flow of 20 mL/min. For the ramp experiments, the reactor was brought to 350 °C and the desired feed mixture (*i.e.,* CH_4/HCl/O_2/N_2/He of 2:2:1:1:14 or 2:16:1:1:0 in mL/min) was fed into the reactor. A stabilization period of 30 min was applied, and then, the ramp experiment of 1 °C/min was commenced at 550 °C. For the stability test, the temperature of the reactor was brought to 450 °C under N_2. After a stabilization period of 15 min, the flow was adjusted to the CH_4/HCl/O_2/N_2/He ratio of 2:2:1:1:14 (in mL/min) and carried out for 10 h. Subsequently, the HCl/He ratio was adjusted, so that the HCl concentration was increased to 20, 40, 60%, and finally 80% HCl, while keeping a constant flow of 20 mL/min. Every feed ratio was tested for 10 h, except for 80% HCl, which was tested for 8 h. During the stability test, *operando* Raman spectroscopy measurements were performed.

The CH_4 conversion, X_{CH_4}, and O_2 conversion, X_{O_2}, are calculated according to eq 1

$$X_a(\%) = \frac{x_{a,inlet} - x_{a,outlet}}{x_{a,inlet}} * 100\% * ISCF \quad (1)$$

where $x_{a,inlet}$, $x_{a,outlet}$, and ISCF stand for the volumetric concentration of compound a at the inlet and outlet of the reactor and the internal standard correction factor, respectively. The yield of product i, Y_i, is calculated according to eq 2

$$Y_i(\%) = \frac{x_i}{x_{CH_4,inlet}} * 100\% * ISCF \quad (2)$$

where x_i and ISCF stand for the volumetric concentration of carbon-containing product i and the internal standard correction factor, respectively. The selectivity of product i, S_i, is calculated according to eq 3.

$$S_i(\%) = \frac{Y_i}{X_{CH_4}} * 100\% \quad (3)$$

The CH_4 reaction rate is calculated according to eq 4

$$R_{CH_4}\left(\frac{mmol}{h * g_{cat}}\right) = \frac{P * F_T * x_{CH_4,inlet} * \frac{X_{CH_4}}{100}}{R * T * W_{cat}} \quad (4)$$

where P, F_T, R, T, and W_{cat} stand for the pressure, total flow, gas constant, ambient temperature, and catalyst weight. Finally, the carbon balance was calculated and measurements with their carbon balance >± 5% were removed. The carbon balance was calculated according to eq 5.

$$\text{Carbon balance} = \sum Y(i) + 100 - X_{CH_4} \quad (5)$$

3. RESULTS AND DISCUSSION

3.1. Catalyst Properties. All synthesized lanthanide oxychloride (LnOCl) materials, made by precipitating $LnCl_3 \cdot xH_2O$ with ammonium hydroxide, were characterized in detail with a battery of analytical methods. The result is a set of solid catalysts with surface areas, crystal phase, and particle morphology in the same order of magnitude. This enables us to study the role of the lanthanide ion within the LnOCl structure and its effect on MOC performances. As an example, Figure 1 shows the XRD patterns of the as-synthesized catalysts.

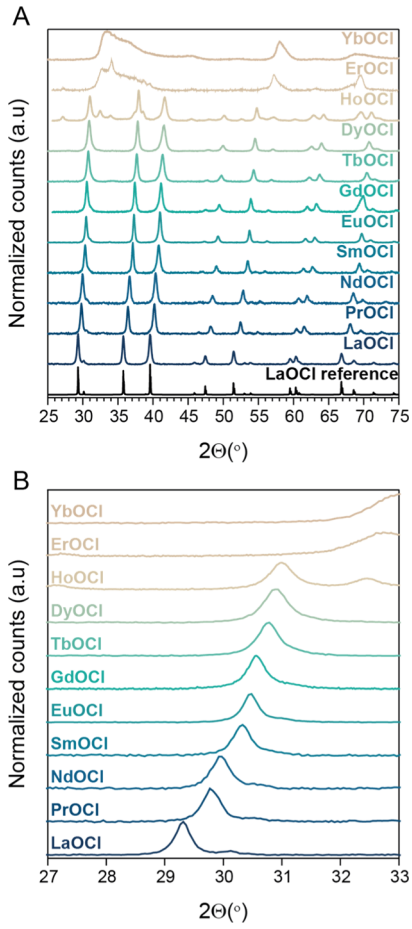

Figure 1. (A) XRD patterns of the catalyst materials under study, including LaOCl, PrOCl, NdOCl, SmOCl, EuOCl, GdOCl, TbOCl, DyOCl, HoOCl, ErOCl, and YbOCl. For each of these materials, they were obtained in their LnOCl phase, except for ErOCl and YbOCl and (B) zoom-in of the XRD patterns, revealing lanthanide contraction in the LnOCl materials, as indicated by the shift of the [101] diffraction in the 27−33° region.

All LnOCl materials have the exact same crystal structure as LaOCl (ICDD 00-00800477). The general trend is that the peak positions (*e.g.,* the [101] diffraction peak) shift toward higher angles with the increasing atom number, as can be concluded from Figure 1B. This reveals a contraction of the lattice parameters, which is caused by the lanthanide contraction effect.[34] Significant contributions of Ho_2O_3 (COD 1537840)

https://doi.org/10.1021/acscatal.1c00393
ACS Catal. 2021, 11, 10574−10588

and Ho_3O_4Cl[35] were observed in the case of HoOCl, but the dominating phase is LnOCl. Unfortunately, for Er and Yb, we were not able to obtain a similar crystal phase, as indicated by the absence of the typical XRD peaks observed for the other LnOCl. In addition, the broadness of the XRD peaks suggests relatively small crystalline domains. For simplicity, we have labeled the Er and Yb catalyst as ErOCl and YbOCl, respectively, although this is formally incorrect.

An overview of the physicochemical properties of the as-synthesized catalysts is given in Table S1. The BET surface area (S_{BET}) within the same order is obtained, albeit we noted some variations, ranging from 15.5 m^2/g (YbOCl) to 50.2 m^2/g (SmOCl). Similarly, the determined pore volume (V_{pore}) ranges from 0.05 cm^3/g (PrOCl) to 0.23 cm^3/g (EuOCl). All the other S_{BET} and V_{pore} values fall within this range and correspond well to the S_{BET} reported for the same synthesis of LaOCl materials by a base precipitation method.[10,17,21,22]

As the catalysts are bulk materials and made with base precipitation, ill-defined particles with a particle size ranging from a few nanometers to hundreds of nanometers are obtained (Figures 2 and S2). Especially for the YbOCl material, smaller particles were absent and only larger irregularly shaped particles were observed (Figure S2).

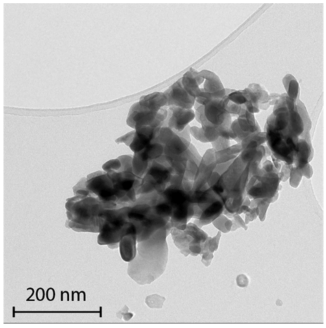

Figure 2. TEM image of the as-synthesized EuOCl where ill-defined particles with varying particle sizes are observed.

The fact that the S_{BET} values (Table S1) are in the same range (15.5−50.2 m^2/g) and that the catalyst materials are synthesized in the same crystal structure, allows us to fairly compare the set of synthesized catalyst materials and study the unique role of the lanthanide element on the activity and selectivity observed in the reaction. HoOCl, ErOCl, and YbOCl do not fully comply with these criteria, but because interesting catalytic behavior was observed, and a complete overview of the lanthanide series could be presented, these catalyst materials are also included in this study.

3.2. Catalytic Performances. The catalytic activity of the as-synthesized lanthanide-based catalyst materials was compared by performing temperature ramp experiments under standard oxychlorination conditions for the production of CH_3Cl. X_{CH_4} and selectivity are plotted *versus* the temperature in Figure 3 for every catalysts individually. The selectivity is plotted when both CH_3Cl and CO were above the detection limit of the GC and the onset temperature at which the catalyst become active is determined as the temperature at which X_{CH_4} > 2%.

All catalysts tested in this study show activity in the MOC reaction. Furthermore, the catalyst materials follow the same trend that X_{CH_4}, S_{CO}, and $S_{CH_2Cl_2}$ increase with the increasing temperature, while S_{CH_3Cl} decreases. Nevertheless, unique catalytic behavior can be observed when comparing the catalyst materials, and large differences in activity and selectivity were observed.

LaOCl, known for its high S_{CH_3Cl},[10,22] becomes active at 480 °C and reaches a maximum X_{CH_4} of 21% at 550 °C. With the increasing temperature, S_{CH_3Cl} decreases from 66 to 32% and S_{CO} increases from 25 to 45%. Substantial amounts of CH_2Cl_2 are formed at 550 °C (S_{CHCl_3} = 18%), while neither CCl_4 nor CO_2 was detected.

PrOCl also becomes active at 480 °C and reaches a maximum X_{CH_4} of 20%. However, the selectivity differs drastically compared to the selectivity obtained with LaOCl. Much of CH_4 is converted to CO, which is the dominant product at temperatures >495 °C. All four CMs can be observed at temperatures >535 °C, albeit in very low concentrations in the case of CCl_4 (S_{CCl_4} < 2%).

For NdOCl, the same onset temperature as for LaOCl and PrOCl was found, namely, 480 °C. However, X_{CH_4} shows a sharp increase in activity from 495 °C to 520 °C (X_{CH_4}: 5% → 16%) after which the activity plateaus till 535 °C. During this sharp increase of X_{CH_4}, the selectivity is also impacted quite drastically as S_{CH_3Cl} decreases from 64 to 38% and S_{CO} is increased from 24 to 38%. Subsequently, X_{CH_4} increases further and reaches a maximum X_{CH_4} of 22%. S_{CH_3Cl} decreases further to 28%, while S_{CO} increases to 46%. $S_{CH_2Cl_2}$ increases gradually from 10 to 19%, while $CHCl_3$ was only detected in minor amounts (S_{CH_3Cl} < 6%).

SmOCl shows higher activity at lower temperatures, as X_{CH_4} > 2% is reached at 465 °C. A gradual increase in the activity is observed up to 550 °C, where it reaches a final X_{CH_4} of 16%. S_{CH_3Cl} decreases from 61 to 30%, while S_{CO} increases from 28 to 46%. $S_{CH_2Cl_2}$ increases with the same trend as S_{CO} from 11 to 20%. $CHCl_3$ was detected in minor amounts (S_{CH_3Cl} < 3%).

The catalytic behavior of EuOCl is unique in a number of aspects. EuOCl shows activity already at low temperatures, as X_{CH_4} > 2% is reached at 385 °C. A maximum X_{CH_4} of 26% is reached at 485 °C, after which X_{CH_4} drops to 19% at 500 °C. Once the temperature further increases, X_{CH_4} steadily increases to the maximum X_{CH_4} of 38%, which is the highest value for all lanthanide-based catalysts tested here under standard oxychlorination conditions. The nature of this drop in X_{CH_4} is discussed in Section 3.4. The unique performance is also reflected in the selectivity plot, where EuOCl has a maximum S_{CH_3Cl} of 75%, which gradually decreases to 29% with the increasing temperature. Both S_{CO} and $S_{CH_2Cl_2}$ increase with the same rate with the increasing temperature, up till the onset of the activity drop at 485 °C. S_{CO} further increases, while $S_{CH_2Cl_2}$ decreases simultaneously up till the end of the drop at 505 °C. From 505 to 550 °C, S_{CO} plateaus at 42%, while $S_{CH_2Cl_2}$ slightly increases to 24%. $CHCl_3$, CCl_4, and CO_2 were all detected, albeit in very low amounts (S_{CHCl_3} < 5%, S_{CCl_4} < 1%, and S_{CO_2} < 2%).

GdOCl, TbOCl, DyOCl, HoOCl, and ErOCl qualitatively show the same trends in activity and selectivity. These catalysts become active at temperatures between 420 and 430 °C, after which X_{CH_4} increases very gradually up to 500 °C. Finally, the

https://doi.org/10.1021/acscatal.1c00393
ACS Catal. 2021, 11, 10574−10588

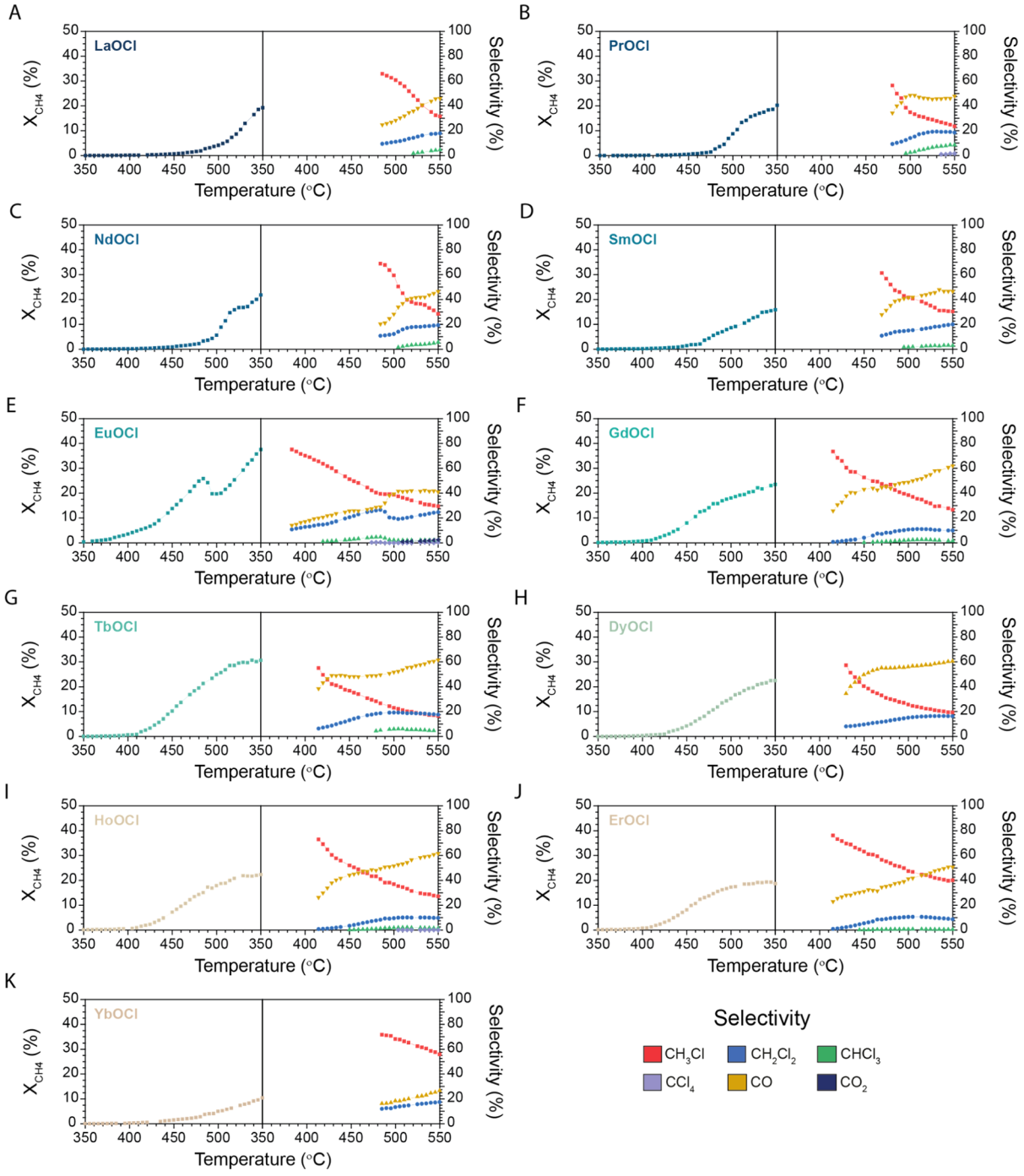

Figure 3. X_{CH_4} and corresponding selectivity plotted *vs* the temperature for LnOCl where Ln = (A) La, (B) Pr, (C) Nd, (D) Sm, (E) Eu, (F) Gd, (G) Tb, (H) Dy, (I) Ho, (J) Er, and (K) Yb. Conditions: $CH_4/HCl/O_2/N_2/He$ of 2:2:1:1:14 (in mL/min) from 350 to 550 °C with a ramp rate of 1 °C/min. Selectivity is given when CH_3Cl and CO were above the detection limit of the GC.

X_{CH_4} increase slightly levels off and reaches the maximum X_{CH_4} at 550 °C. For GdOCl, TbOCl, DyOCl, HoOCl, and ErOCl, the maximum X_{CH_4} is 23, 30, 26, 22, and 19%, respectively. Furthermore, these catalysts show similar selectivity profiles. S_{CH_3Cl} steadily decreases over the tested temperature range, with the best performance for ErOCl (S_{CH_3Cl} 76% → 40%) and the worst performance for DyOCl (S_{CH_3Cl} 55% → 16%). S_{CO} first sharply increases up till ∼440 °C and then gradually increases to an S_{CO} of 51−62% with the best performance again for ErOCl. $S_{CH_2Cl_2}$ increases up till ∼500 °C after which it levels off/slightly decreases and reaches a final $S_{CH_2Cl_2}$ of 10−20%. $CHCl_3$ was only detected in reasonable amounts for TbOCl and did not increase above 6% over the tested temperature range. CCl_4 and CO_2 were not detected.

Lastly, YbOCl shows relatively low overall activity, as X_{CH_4} > 2% is reached at 465 °C and reaches a maximum X_{CH_4} of 11%. S_{CH_3Cl} decreases from 72 to 56%, and S_{CO} increases from 16 to 26%. Furthermore, only CH_2Cl_2 is detected, which grows from

https://doi.org/10.1021/acscatal.1c00393
ACS Catal. 2021, 11, 10574−10588

12 to 18%. No higher CMs were observed, and no CO_2 was detected.

The CH_4 conversion rate and the corresponding selectivity for every catalyst material tested in this study at a temperature of 480 °C are plotted in Figure 4. This comparative plot clearly

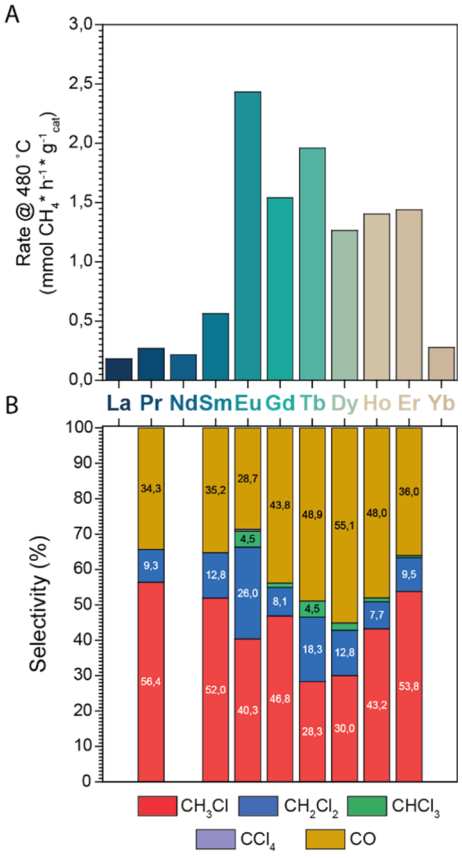

Figure 4. (A) CH_4 conversion rate and (B) selectivity toward CH_3Cl, CH_2Cl_2, $CHCl_3$, CCl_4, and CO for LnOCl (with Ln = La, Pr, Nd, Sm, Eu, Gd, Tb, Dy, Ho, Er, or Yb) at a reaction temperature of 480 °C. Note that for LaOCl, NdOCl, and YbOCl, the CO yield was below the detection limit, and therefore, the selectivity is not displayed. For all catalysts, the CO_2 levels were below the detection limit.

shows that, even though the catalysts are chemically and physically comparable, large differences in both the activity and selectivity are induced by the lanthanide element. The highest CH_4 conversion rate of 2.43 mmol $CH_4{*}h^{-1}{*}g^{-1}_{cat}$ was observed for EuOCl, which is ~13× times higher than that for LaOCl. Based on the CH_4 conversion rate, the following activity ranking was found: Eu > Tb > Gd ~ Ho ~ Er > Dy > Sm > Pr ≈ Nd ≈ La ≈ Yb with a maximum X_{CH_4} of 24% for EuOCl and a minimum X_{CH_4} of 2% for LaOCl (Figure 4). A similar ranking can be constructed based on S_{CO} (Eu > Pr ~ Sm ~ Er > Gd > Ho ~ Tb > Dy) and $S_{CH_3Cl + CH_2Cl_2}$ (Eu ~ Pr ~ Sm ~ Er > Gd > Ho ~ Tb > Dy) at 480 °C. La, Nd, and Yb are not considered with the selectivity ranking, as the CO yield was below the detection level.

Based on the activity and selectivity performance, EuOCl shows the most promising catalytic behavior, as the highest X_{CH_4} and the best selectivity at reasonable conversion levels are found. Interestingly, LaOCl is often reported for its high S_{CH_3Cl} at reasonable conversion levels, but compared to the other lanthanide catalysts tested, its catalytic performance is mediocre under the reaction conditions applied here.[10,11,22]

Based on the abovementioned experimental findings, it is important to better understand the parameters that tune the reaction selectivity. Four key processes occurring during the MOC reaction for LnOCl materials are schematically depicted in Figure 5. These four processes, namely, the oxychlorination of C_1 (arrows 1−4),[21] a possible pathway for the catalytic destruction of CR_2Cl_2 (arrows 5−8),[33,36] chlorination of terminal lattice oxygen (arrow 9), and bulk diffusion of O/Cl (arrow 10), are connected, as they transition over the same surface compositions. The premise is to skip the catalytic destruction cycle and accelerate the oxychlorination cycle. In the catalytic chlorination of methane, surface chlorination *via* HCl plays a crucial role. Surface hydroxyl groups react with HCl to form surface chlorine and H_2O (arrows 1−2). The surface hydroxyl groups regenerated as C_1 and O_2 react over the surface chlorine (arrows 3−4). However, the oxychlorination cycle can be skipped, once terminal lattice oxygen is formed *via* condensation *via* the hydrolysis of surface hydroxyl groups (arrow 5).[37] The catalytic destruction of CMs over terminal lattice oxygen of La is well described,[38] and it is hypothesized that a similar mechanism plays a role for the lanthanide-based catalysts tested in this study. When the CM catalytically destructs (arrows 6−7), surface chlorination is again obtained, where it crosses paths with the oxychlorination cycle again. H_2O formed during the oxychlorination reaction and surface condensation can react with the formed surface chlorine, regenerating the surface hydroxyl groups (arrow 8). Important to note is that terminal lattice oxygen, over which catalytic destruction of CMs can occur, can either be chlorinated with HCl (arrow 9) or exchanged with mobile bulk chlorine (arrow 10). In the case of nonsteady state behavior of the catalyst composition, bulk diffusion of ions is partly accountable for changing catalyst surface compositions.[38] Pivotal in the envisaged reaction cycles is the regeneration of the surface chlorine on which MOC can occur and the catalytic destruction of CMs is prevented.

A direct way to influence the degree of surface chlorination is by altering the HCl concentration under isothermal conditions. To investigate this effect, the catalysts were brought to X_{CH_4} ≈ 10% and the concentration of HCl in the feed was increased. X_{CH_4}, S_{CH_3Cl}, S_{CO}, and $S_{CH_2Cl_2}$ are shown in Figure 6, while S_{CHCl_3} and S_{CCl_4} can be found in Figure S3. Generally, four types of responses can be identified for the different catalyst materials tested on the basis of their measured X_{CH_4} values: (1) increased activity (Figure 6, first row), (2) steady activity (Figure 6, second row), (3) slowly decaying activity (Figure 6, third row), and (4) instantaneous deactivation (Figure 6, bottom row).

We ascribe EuOCl to the first category; increased activity with the increasing HCl concentration. X_{CH_4} is increased from 11 to 25% going from 10 to 60% HCl in the gas feed. Thereafter, the activity seems to plateau up to 80% HCl. The increase in HCl concentration does not only boost the activity but also suppresses S_{CO} from 28 to 14%. Furthermore, S_{CH_3Cl} decreases slightly, while $S_{CH_2Cl_2}$ and S_{CHCl_3} increase with the increasing HCl concentration. The formation of CO is largely caused by the catalytic destruction of CH_2Cl_2 and $CHCl_3$, as S_{CO} and $S_{CH_2Cl_2}/S_{CHCl_3}$ are negatively correlated. The prevention of the catalytic

https://doi.org/10.1021/acscatal.1c00393
ACS Catal. 2021, 11, 10574−10588

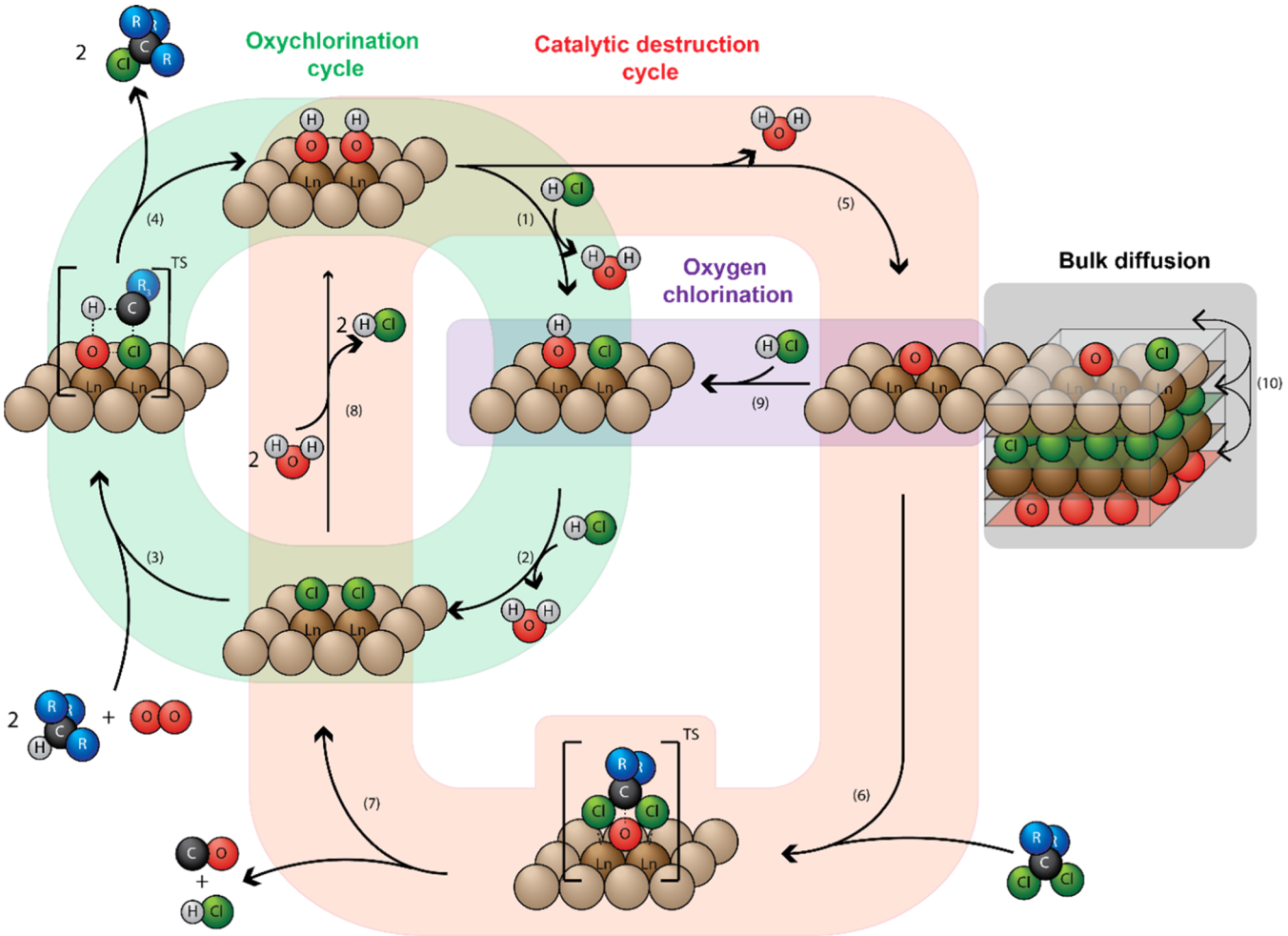

Figure 5. Schematic representation of relevant processes occurring during the MOC reaction over LnOCl materials. The oxychlorination cycle (green, arrows 1−4) and catalytic destruction cycle (red, arrows 5−8) are in competition with one another. The chlorination of terminal lattice oxygen (purple, arrow 9) is an important step because terminal lattice oxygen is held responsible for the catalytic destruction of higher chloromethanes. The surface composition is determined not only by the reactants but also by bulk diffusion of ions (gray, arrow 10).

destruction of higher CMs is evidenced by the observed S_{CCl_4} for EuOCl. The increase in HCl concentration thus has a double-sided effect: (1) less surface oxygen where higher CMs can be catalytically destructed on and (2) the generation of more active sites where chlorination of C_1 can occur. Carefully choosing the $CH_4/HCl/O_2$ ratio is thus of great importance for optimal catalytic activity.

SmOCl, DyOCl, and YbOCl show similar activity response with the increasing HCl concentration, although the exact values differ significantly. Their X_{CH_4} is rather insensitive to the HCl concentration in the feed and only increases slightly. S_{CH_3Cl} and S_{CO} slightly decrease or remain constant, which is in line with X_{CH_4}. S_{CHCl_3} seems inversely proportional to S_{CO} and S_{CH_3Cl} for DyOCl and YbOCl because it shows an upward trend with the increasing HCl concentration (Figure S3A). For SmOCl, no formation of CH_3Cl was observed, indicating that no CH_3Cl was formed or that all formed $CHCl_3$ was destructed. For these catalyst materials, S_{CO} could not be suppressed as dramatically as for EuOCl (for DyOCl 49% → 37% *vs* for EuOCl 29% → 14%). A higher degree of surface chlorination mainly results in preventing the catalytic destruction of higher CMs for DyOCl and YbOCl, and to a lesser extent, the generation of more active sites for all three catalysts. The generation of more active sites did not result in a higher X_{CH_4} but in a higher overall degree of chlorination of methane. The reactivity of C_1 increases with the increasing chlorine content,[21] and it appears that CH_4 and the other CMs are in competition over the same active site(s).

LaOCl, GdOCl, TbOCl, HoOCl, and ErOCl all show a decaying activity profile with the increasing HCl concentration in the feed. The activity drops the most for TbOCl (X_{CH_4} 12% → 4%) and the least for LaOCl (X_{CH_4} 10%→ 7%). When further comparing these five catalysts based on their selectivity, LaOCl and ErOCl show very similar behavior and GdOCl, TbOCl, and HoOCl show very similar behavior. While X_{CH_4} of LaOCl and ErOCl decreases gradually, S_{CH_3Cl}, S_{CO}, and $S_{CH_2Cl_2}$ are not significantly affected. The largest difference in selectivity of these two catalysts can be observed for LaOCl where S_{CH_3Cl} is reduced by 7%. The higher HCl concentration causes CH_3Cl to be further chlorinated to CH_2Cl_2. The additional CH_2Cl_2 is catalytically destructed, either directly or indirectly *via* the formation of $CHCl_3$. For GdOCl, TbOCl, and HoOCl, however, larger differences in selectivity are observed, as S_{CO} decreases from 51 to 33% for TbOCl, while S_{CH_3Cl} simultaneously increases from 33 to 52%. GdOCl, TbOCl, and HoOCl are the only catalysts that show an increase in S_{CH_3Cl} with the

https://doi.org/10.1021/acscatal.1c00393
ACS Catal. 2021, 11, 10574−10588

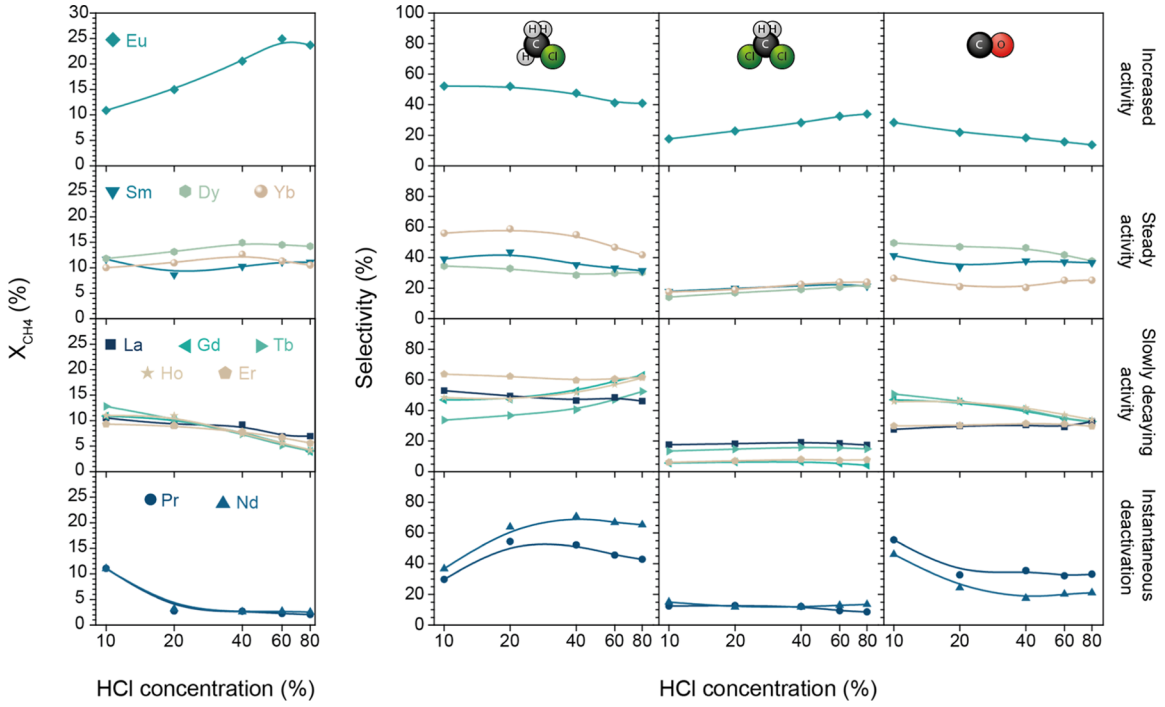

Figure 6. X_{CH_4}, S_{CH_3Cl}, $S_{CH_2Cl_2}$, and S_{CO} over LnOCl materials (with Ln = La, Pr, Nd, Sm, Eu, Gd, Tb, Dy, Ho, Er, or Yb) plotted *vs* the HCl concentration for the four different categories of catalytic behavior under study. The elements with their corresponding symbol are displayed in the X_{CH_4}−HCl concentration plot.

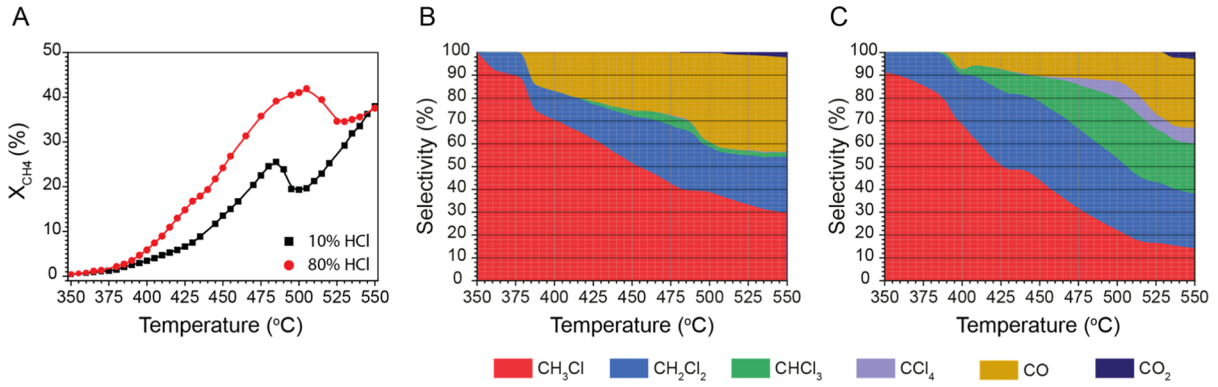

Figure 7. (A) X_{CH_4} plotted *vs* the temperature for EuOCl under 10% (black) and 80% (red) HCl. Selectivity toward CH_3Cl, CH_2Cl_2, $CHCl_3$, CCl_4, CO, and CO_2 is plotted *versus* the temperature for EuOCl tested in (A) 10% HCl (CH_4/HCl/O_2/N_2/He 2:2:1:1:14) and (B) 80% HCl (CH_4/HCl/O_2/N_2/He 2:16:1:1:0).

increasing HCl concentration. The lower X_{CH_4} causes less $CHCl_3$ to form (Figure S3A), which is subsequently destructed to CO. The lower activity also affects the degree of methane chlorination and thus lowers the quantity of higher CMs present in the system that can be destructed.[33,36]

PrOCl and NdOCl fall within the last category having a catalytic activity that is almost completely lost with the increasing HCl concentration. As the activity is correlated to the selectivity observed in the reaction, we observe that S_{CH_3Cl} drastically increases. However, X_{CH_4} (<5%) is too low for commercial use and, therefore, the selectivity observed is irrelevant. The nature of this rapid X_{CH_4} decrease is not investigated in this study, but it is hypothesized that a completely chlorinated surface inhibits the activation of O_2 and/or CH_4 by a change in material acidity/basicity.

Unlike the other catalyst materials tested in this study, the catalytic performance of EuOCl can be steered by tuning two key parameters, namely, temperature and HCl concentration. The extreme HCl concentrations applied in this study, 10 and 80%, are compared in the temperature range of 350−550 °C. X_{CH_4} of EuOCl is plotted *versus* the temperature, as shown in Figure 7A, for the two tested HCl concentrations. Immediately visible is the enhancement of activity from the HCl increase over the entire tested temperature range. Under 10% HCl, the maximum X_{CH_4} of 38% is reached at 550 °C. The increase in HCl concentration simultaneously lowers the temperature at which the maximum X_{CH_4} is reached to 505 °C and increases the max X_{CH_4} to 42%. Furthermore, the observed activity drop is delayed by 20 °C; the nature of this drop will be discussed in Section 3.4. To further demonstrate the remarkable activity increase of

https://doi.org/10.1021/acscatal.1c00393
ACS Catal. 2021, 11, 10574−10588

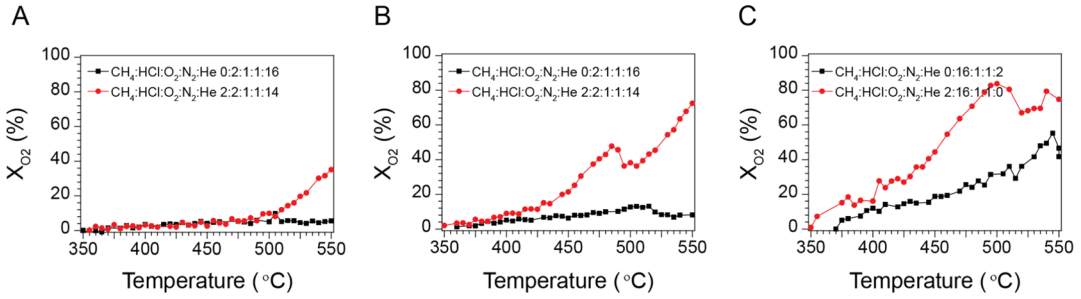

Figure 8. Temperature ramp experiments where X_{O_2} is plotted *vs* the temperature for HCl oxidation reaction (black) and MOC (red) for (A) LaOCl with 10% HCl in the feed, (B) EuOCl with 10% HCl in the feed, and (C) EuOCl with 80% HCl in the feed.

EuOCl upon increasing the HCl concentration, X_{CH_4} is plotted *versus* the temperature for all catalyst materials at a HCl concentration of 10 and 80%, as shown in Figure S4A,B, respectively. Except for EuOCl, X_{CH_4} of all catalysts was negatively influenced by the increase in HCl concentration over the entire temperature range. This coincides with the results presented in Figure 6, where EuOCl was the only catalyst that showed an increase in X_{CH_4} when increasing the HCl concentration. The maximum X_{CH_4} of all catalysts dropped significantly, for example, from 31 to 19% for TbOCl.

When further comparing the temperature-dependent performance of EuOCl at 10 and 80% HCl concentration, large selectivity differences are observed (Figure 7B,C). S_{CO} is suppressed below 15% at 80% HCl, even at very high conversion levels (X_{CH_4} = ~40%). To our best knowledge, such a low CO selectivity at high conversion levels is yet unreported and makes the EuOCl material in this study a potential catalyst material for practical applications. The result of the lower CO selectivity is an increase in selectivity toward higher CMs. At 80% HCl concentration and 475 °C, all four CMs are produced. One major drawback from operating the EuOCl system at such high conversion levels is that the selectivity toward CH_3Cl drastically decreases. The generation of more active sites by fast chlorination due to the excess HCl causes the formed CH_3Cl to react further to higher CMs. In that regard, the HCl concentration does not have a significant effect on the CH_3Cl selectivity when comparing two different ratios. At 10% conversion, both ratios have S_{CH_3Cl} = ~60% at X_{CH_4} = 10%. CO_2 was only detected at high temperatures (>500 °C), and the selectivity was very low (<1.2%).

With such large formations of CH_2Cl_2 and $CHCl_3$ and noticeable amounts of CCl_4 observed at high conversion levels at 80% HCl, thermal chlorination might be a viable route instead of surface-catalyzed reaction. This is supported by the fact that a discrepancy in the product selectivity was observed when comparing 10 and 80% HCl in the feed (Figure 7B,C). A previous work by Pérez-Ramírez and co-workers already investigated the HCl oxidation over EuOCl.[6] Based on these findings, the thermal chlorination of methane with Cl_2 seems to only have a minor contribution to the total chlorination of methane at the used temperature range in this study. However, the reaction mechanism proposed for LaOCl does not explain how such a high selectivity toward, for example, $CHCl_3$ can be obtained as observed for EuOCl. A previous work by our group already proposed a mechanism where La is shortly reduced by accepting a H from CH_2Cl_2.[33] The proven presence of the redox couple Eu^{2+}/Eu^{3+} could participate in the reaction *via* a similar role, and a mechanism can be proposed for EuOCl where Eu changes the oxidation state during the reaction.[39] Furthermore, the presence of substantial amounts of Eu^{2+} was proven under oxychlorination conditions at $T > 753$ K. To investigate what the contribution of the gas-phase chlorination of methane is to the total catalytic performance of LaOCl and EuOCl, the oxygen conversion (X_{O_2}) was determined in a reaction mixture with and without the presence of CH_4. The HCl oxidation results are compared to the oxychlorination reaction with the same HCl/O_2 feed ratio. For LaOCl (Figure 8A), X_{O_2} was below 5% over the entire tested temperature range. For the oxychlorination reaction over LaOCl, a sharp increase in X_{O_2} is observed from 500 to 550 °C, where X_{O_2} reaches a final value of 35%. As expected from the literature, no Cl_2 seems to evolve, and thus, the gas-phase chlorination of methane does not contribute to the overall activity of LaOCl.[10] HCl oxidation over EuOCl was tested at 10 and 80% HCl in the feed (Figure 8B,C respectively), as large differences in activity and selectivity were observed when the HCl concentration was varied. At 10% HCl in the feed, X_{O_2} for the oxychlorination reaction is significantly higher than that for the HCl oxidation over the entire temperature range. However, some consumption of O_2 is visible for the HCl oxidation with a maximum X_{O_2} of 13%, thus contributing to the overall performance, although the activity and selectivity are predominantly governed by the surface-catalyzed reaction. The discrepancy between X_{O_2} of the HCl oxidation and MOC reaction is reduced when the HCl concentration is increased to 80%. X_{O_2} of both reactions increased, and the relative difference is decreased. Solely by increasing the HCl concentration, the maximum X_{O_2} is enhanced from 13 to 55% for the HCl oxidation reaction. The HCl oxidation reaction is accelerated by the large excess of chlorine present on/in the catalyst, and HCl oxidation plays a major role in the overall performance of the catalyst. The large difference in HCl oxidation potency at 10 and 80% HCl also partly explains why the degree of methane chlorination is enhanced when a high HCl concentration is used.

The total product selectivity here is partly governed by the free radical reaction, which offers very limited control over the selectivity.[16,45] Further research is needed to investigate if the reducibility of Eu^{3+} is enhanced by the excess of HCl. Up till so far, we have demonstrated the excellent performance of EuOCl and compared it to the other catalyst materials reported in this study. However, the reducible CeO_2 is arguably the best performing catalyst in MOC with a combined yield of CH_3Cl and CH_2Cl_2 of ~27%.[14] For EuOCl, a remarkable maximum combined yield of 24% is obtained at 485 °C at 80% HCl. We

https://doi.org/10.1021/acscatal.1c00393
ACS Catal. 2021, 11, 10574−10588

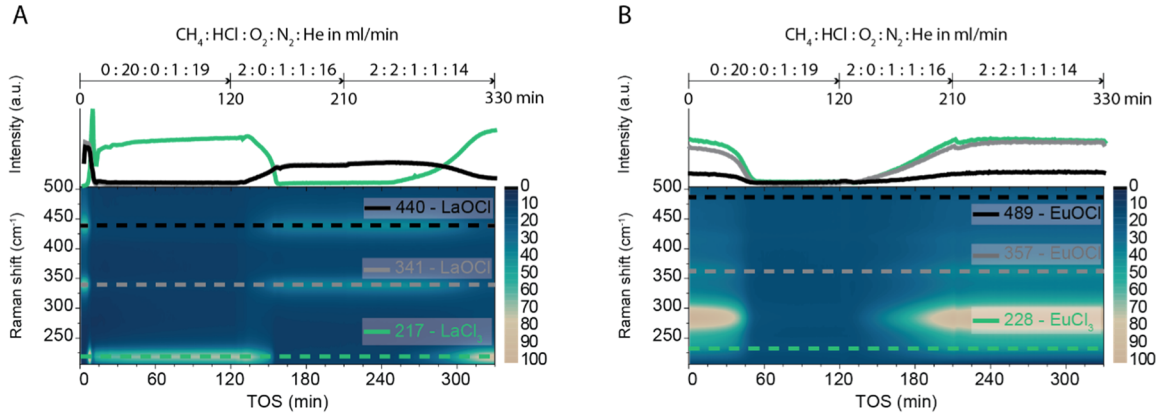

Figure 9. Chlorination (minute 0−120, $CH_4/HCl/O_2/N_2/He$ 0:20:0:1:19, T = 450 °C), dechlorination (minute 120−210, $CH_4/HCl/O_2/N_2/He$ 2:0:1:1:16, T = 500 °C), and oxychlorination (minute 210−330, $CH_4/HCl/O_2/N_2/He$ 2:2:1:1:14, T = 500 °C) steps were investigated with *operando* Raman spectroscopy for (A) LaOCl and (B) EuOCl materials. The Raman spectra are plotted as contour plots, and the intensity of key vibrations is plotted above. For 3-D plots and individual spectra, see Figure S6.

hypothesize that by altering the reducibility,[46] enhancing the surface area of the active phase,[22,47] and/or increasing the rate of chlorination by adding additives, the benchmark performance of CeO_2 can be matched and potentially exceeded.

Lastly, the response to the change in HCl concentration in the MOC reaction differs quite drastically from one lanthanide material to another. For catalysts that have the same chemical composition (*e.g.*, supported catalysts with different particle sizes), S_{BET} of the active phase is often correlated to an increase in activity.[48,49] However, in this study, the element is varied, while the physical properties of the materials are kept within the same order. To evaluate whether the activity is correlated to S_{BET}, the as-synthesized S_{BET} was taken and correlated to the temperature, where X_{CH_4} = 10% at 10% HCl flow (Figure S5). The calculated R^2 was negative, indicating that there is no correlation between the activity of the various lanthanide materials and S_{BET}. Thus, the difference in catalytic performance is due to the unique properties of the lanthanide element. Correlating the activity to physical properties of lanthanide-based catalyst materials was attempted in the literature for oxychlorination[22] and C_1 catalytic destruction,[33,38,47] but this did not yield conclusive results. Due to the fact that the oxychlorination reaction is composed of two noncatalytic reactions coupled in a catalytic cycle, we must also study the catalyst condition because a more complex mechanism is most probably present that determines the catalyst performance.

3.3. *Operando* Raman Spectroscopy. In the next stage of our study, we have performed *operando* Raman spectroscopy to study the occurring phase changes during the chlorination, dechlorination, and oxychlorination reactions of LaOCl and EuOCl. The chlorination and dechlorination steps are studied separately, as both steps occur simultaneously and form the catalytic cycle of MOC. LaOCl and EuOCl were selected, as EuOCl shows the most promising catalytic performance of the catalysts tested in this study and LaOCl is often reported for its high S_{CH_3Cl} at reasonable conversion levels.[10,11,22] Moreover, both catalysts react differently to a changing HCl concentration in the feed, and hence, detailed characterization studies could provide further insights into the differences between both systems. The results of the *operando* Raman study are shown in Figure 9. The corresponding Raman spectra are 3-D plotted in Figure S6A,C for LaOCl and EuOCl, respectively. Individual spectra with 60 min time intervals are given in Figure S6B,D for LaOCl and EuOCl materials, respectively. The band attribution is summarized in Table 1.

Table 1. Frequencies in Raman Shift (cm^{-1}) of Raman Vibrational Modes Observable for LaOCl, EuOCl, $LaCl_3$, and $EuCl_3$

	E_g	A_{1g}	E_g	A_{1g}, B_{2g}	E_g	refs
LaOCl	125	189	215	336	441	40,41
EuOCl	120	182	235	357	489	42,43
	E_{2g}	A_g	E_{1g}	$2E_{2g} + A_g$		refs
$LaCl_3$	110	179	185	208 & 213		41,44
$EuCl_3$	95	184	198	228		44

The spectral data of LaOCl is visualized as a contour plot in Figure 9A. Above the contour plot, the intensity plot of three characteristic vibrations, that is, 217 cm^{-1} ($2E_{2g} + A_g$ of $LaCl_3$), 341 cm^{-1} (A_{1g}, B_{2g} of LaOCl), and 440 cm^{-1} (E_g of LaOCl) is plotted *versus* time on stream. From 0−120 min, the catalyst is chlorinated ($CH_4/HCl/O_2/N_2/He$ 0:20:0:1:19 in mL/min) at 450 °C. The fresh LaOCl is rapidly converted into $LaCl_3$ because A_{1g}/B_{2g} and E_g of LaOCl disappears within several minutes, while $2E_{2g} + A_g$ of $LaCl_3$ shows the opposite trend. The intensity of the vibrational modes corresponding to LaOCl do not change significantly after 10 min and disappear in the background. The intensity decrease of the LaOCl vibrational modes and the growth of the $LaCl_3$ vibrational mode at 217 cm^{-1} occur simultaneously. A rapid increase in peak intensity is observed within the first 10 min after which the Raman vibration intensity growth levels off, as can be seen in the intensity plot. This indicates that LaOCl is almost fully converted into $LaCl_3$ within 15 min of chlorination. From 120−210 min, the catalyst was first heated to 500 °C and a dechlorination step ($CH_4/HCl/O_2/N_2/He$ 2:0:1:1:16) was performed. The dechlorination of the catalyst material was complete after 155 min because A_{1g}/B_{2g} and E_g of LaOCl reach their final value and $2E_{2g} + A_g$ of $LaCl_3$ disappears in the background. No Raman vibration at 408 cm^{-1}, corresponding to La_2O_3, was observed.[41,47] From 210−330 min, a typical oxychlorination reaction mixture ($CH_4/HCl/O_2/N_2/He$ 2:2:1:1:14) was fed into the reactor at 500 °C. No observable spectral changes occur from 210−245 min, which is most probably caused by the probed catalyst bed height. It is hypothesized that HCl is completely consumed by the top of the

https://doi.org/10.1021/acscatal.1c00393
ACS Catal. 2021, 11, 10574−10588

catalyst bed before a steady-state consumption of HCl is reached and HCl travels further through the catalyst bed. Here, a more gradual transition between LaOCl to $LaCl_3$ is observed, starting after 270 min. As already expected from the chlorination and dechlorination steps, the rate of chlorination exceeds the rate of dechlorination. After 330 min, vibrational modes corresponding to LaOCl and $LaCl_3$ are both visible, indicating that the catalyst material is in between a LaOCl−$LaCl_3$ state. However, at the end of the experiment, the intensity of the LaOCl bands almost disappeared in the background (Figure S6B). At 330 min, the catalyst is composed of almost pure $LaCl_3$ and it is expected that the remaining LaOCl would be converted to $LaCl_3$ over prolonged reaction times. Thus, even at low HCl concentrations (10%), the chlorination rate of the catalyst material exceeds the dechlorination rate.

The same chlorination−dechlorination−oxychlorination experiment was performed for the EuOCl material. The spectral data of EuOCl are visualized as a contour plot in Figure 9B. Above the contour plot, the intensity of three vibrations at 228 cm^{-1} ($2E_{2g}$ + A_g of $EuCl_3$), 357 cm^{-1} (A_{1g}, B_{2g} of EuOCl), and 489 cm^{-1} (E_g of EuOCl) is plotted *versus* the time on stream. In the Raman spectrum of EuOCl, two bands at 282 cm^{-1} (λ = 540 nm) and 423 cm^{-1} (λ = 544 nm) cannot be ascribed to Raman vibrations. These peaks most likely correspond to the $^5D_1 \rightarrow {}^7F_{0-2}$ (λ = 525−584 nm) emission lines of Eu^{3+}.[50,51] From 0−120 min, a gradual decrease of all Raman vibration intensities is observed and it appears that the final state is only reached after 50 min of reaction. Considering that LaOCl was fully chlorinated to $LaCl_3$ within 15 min, it can be stated that EuOCl is less susceptible to chlorinate into $LnCl_3$ than LaOCl. The typical vibration of $EuCl_3$ at 228 cm^{-1} also decreases in intensity because it overlaps with the more intense 282 cm^{-1} emission line, which decreases over time. The observed intensity of the $EuCl_3$ vibration at the tested temperature is very weak (Figure S6D), probably due to the weakening of the Eu−Cl bond and the loss of coordination number near T_{melt}.[44] Not only is the Raman signal lost upon chlorination, but the photoluminescence signal of $EuCl_3$ is also quenched upon heating. In Figure S7A,B, a temperature ramp on EuOCl/$EuCl_3$ was performed. A gradual change from the $EuCl_3$ spectrum to the EuOCl spectrum is observed, heating from 20 to 350 °C. No difference can be observed between the reference EuOCl and the EuOCl/$EuCl_3$ spectrum (Figure S7C), even though the composition of the heated sample did not change during the temperature ramp (Figure S7D). The loss of the signal, both in the Raman and photoluminescence spectra, indicates the chlorination of EuOCl to $EuCl_3$. Hence, the photoluminescence intensity is directly correlated to the degree of catalyst chlorination. From 120−210 min, the intensity of all Raman bands is restored during the dechlorination. Again, the Raman signal of the $2E_{2g}$ + A_g vibration of $EuCl_3$ at 235 cm^{-1} increases due to the rise of the relatively broad 282 cm^{-1} emission line. No formation of Eu_2O_3 was observed, as its distinct vibration at 345 cm^{-1} was not detected.[52,53] From 210−330 min, the Raman spectra did not change during the oxychlorination step. A small variation in peak intensity was observed in the beginning of the experiment, but from the intensity plot, it is apparent that no major changes occurred. Hence, little bulk chlorination takes place. The high rate of methane chlorination, and thus surface dechlorination, results in that EuOCl does not bulk chlorinate. Evident from the reaction mechanism (Figure 5) is that the surface chlorination must occur for the reaction to take place. In combination with the fact that the activity is increased with the increasing HCl concentration, we can conclude that the surface chlorination is rate-limiting and not the activation of O_2 or CH_4. An increase in the HCl concentration is therefore beneficial for the catalytic activity of EuOCl because surface chlorination occurs more readily.

3.4. *Operando* Photoluminescence Spectroscopy. Both activity profiles of EuOCl shown in Figure 7A show a similar behavior, as both profiles show a drop in the activity after which the activity is restored at higher temperatures. At 10% HCl, the onset of the drop occurs at ∼475 °C and the minimum is reached at ∼500 °C. At 80% HCl, the onset of the drop is delayed from 480 to 500 °C and a maximum X_{CH_4} of 42% is reached. At 550 °C, EuOCl reaches the same X_{CH_4} of ∼38% for both conditions. As this drop is reproducible with different newly synthesized EuOCl catalysts and for the same EuOCl catalyst when the same experiment is repeated, we investigated the role of the degree of catalyst chlorination on the drop in activity. Temperature ramp experiments from 450 to 520 °C were performed with the same catalyst, but the pretreatment step was varied. Furthermore, photoluminescence spectra of EuOCl were collected with the *operando* Raman probe. The collected spectra were normalized to the highest signal of the series and integrated over the entire spectral range. The relative spectral area is used as a measure for the degree of chlorination, as the chlorination of EuOCl to $EuCl_3$ quenches the signal, as described in Section 3.3. The X_{CH_4} and relative spectral area are plotted *versus* the temperature. In Figure 10A, standard oxychlorination at 450 °C was applied as a pretreatment step (CH_4/HCl/O_2/N_2/He 2:2:1:1:14). X_{CH_4} increases linearly with

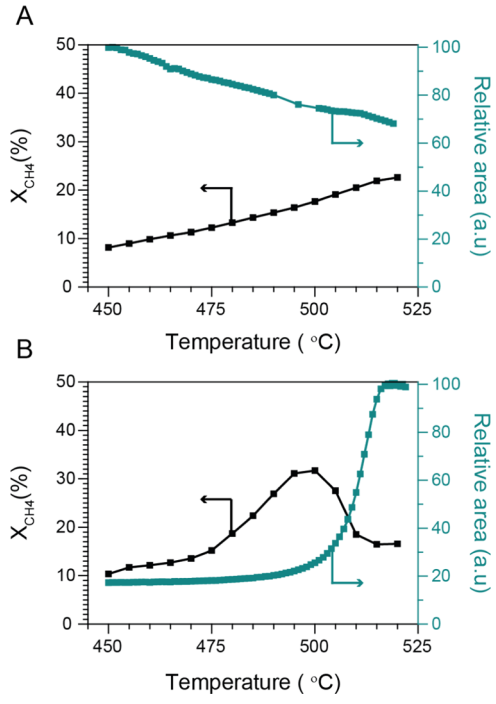

Figure 10. Temperature ramp experiments between 450 and 520 °C at 1 °C/min for EuOCl at the CH_4/HCl/O_2/N_2/He ratio of 2:2:1:1:14 with 2 h pretreatment of (A) CH_4/HCl/O_2/N_2/He 2:2:1:1:14 at 450 °C and (B) CH_4/HCl/O_2/N_2/He 0:4:0:1:15 at 450 °C. The photoluminescence spectra were collected, normalized to the highest peak, and integrated. The relative spectral area and X_{CH_4} were plotted *vs* the temperature.

https://doi.org/10.1021/acscatal.1c00393
ACS Catal. 2021, 11, 10574−10588

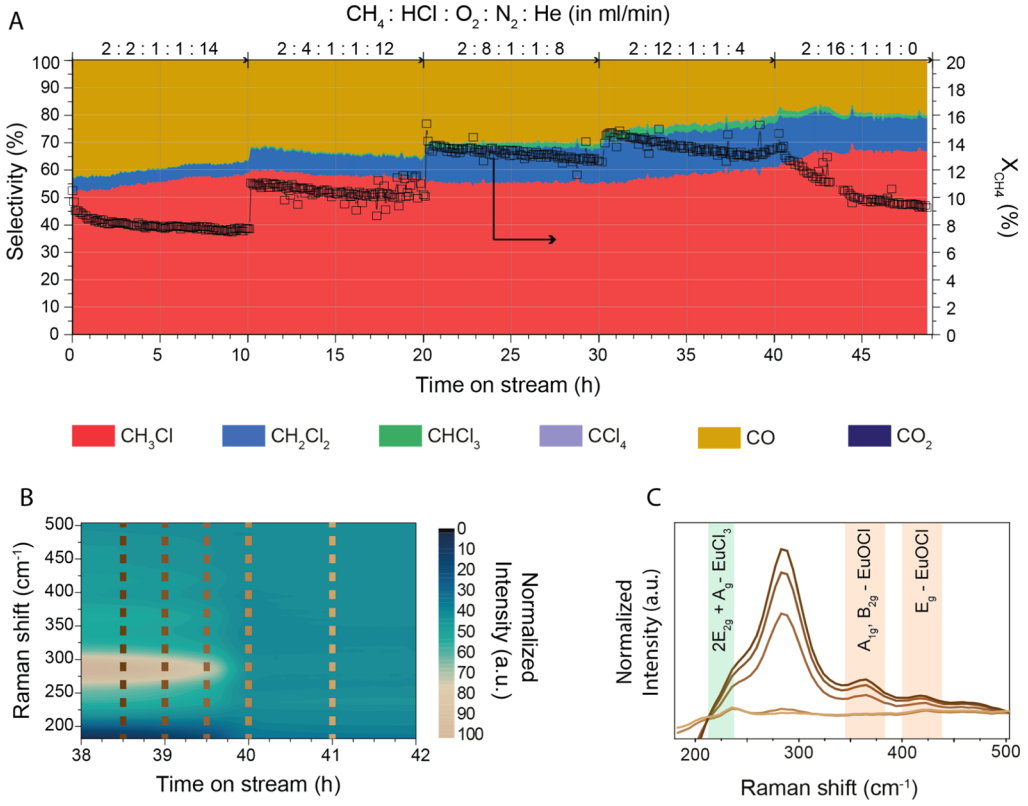

Figure 11. (A) X_{CH_4} and S_{CH_3Cl}, $S_{CH_2Cl_2}$, S_{CHCl_3}, S_{CCl_4}, S_{CO}, and S_{CO_2} plotted *vs* time on stream and (B) *operando* Raman spectra plotted *vs* time on stream between 38 and 42 h. The vertical lines in (B) are plotted individually in (C) to show the loss of Raman peak intensity of the vibrations corresponding to EuOCl.

the increasing temperature, while the opposite trend is observed for the relative spectral area. No spectral changes occurred during the temperature ramp, and only the intensity of the signal decreased with the increasing temperature. The gradual decrease in the relative area is expected, as the overall photoluminescence intensity is negatively correlated with the temperature. Subsequently, the catalyst was cooled to 450 °C and chlorinated for 2 h prior to the temperature ramp (CH_4/HCl/O_2/N_2/He 0:4:0:1:15), as shown in Figure 10B. Now, the drop in activity is observed, starting at 500 °C, which coincides with the temperature of the drop observed in Figure 7A for EuOCl tested at 80% HCl. The sharp decrease in activity and the exponential growth of the relative spectral area occur simultaneously, indicating that bulk $EuCl_3$ is rapidly converted to EuOCl, as mostly the state of the catalyst bulk is probed with photoluminescence spectroscopy. Both X_{CH_4} and the relative spectral area stabilize at 515 °C, indicating that the catalyst reaches a steady state. The reaction temperature plays a crucial role in the degree of catalyst chlorination. In a scenario where excess HCl is present in the feed, bulk chlorination occurs at lower temperatures. Once the temperature is increased to >480 °C, bulk chlorination becomes unfavorable, and the bulk chlorine migrates to the surface, temporarily increasing the degree of surface chlorination. Hence, an increase in the activity is observed, as chlorine is forced out of the catalyst. Once the free chlorine in the catalyst depletes, activity and selectivity are restored to the same levels as observed when no drop in activity was observed. The pretreatment step as shown in Figure 10A,B additionally reveals that the presence of methane also plays a vital role in the degree of catalyst chlorination. Figure 8B shows that the HCl oxidation rate at 450 °C and 10% HCl is low, and dechlorination of the catalyst *via* HCl oxidation is thus a slow process. Furthermore, the HCl oxidation rate is limited by the HCl concentration in the feed, as the rate could be significantly enhanced when excess HCl was fed (Figure 8C). In Figure 10, we showcase that with and without the presence of methane in the feed, the catalyst is either in a dechlorinated or in a chlorinated state, respectively. We can therefore conclude that the state of the catalyst is determined by both the reaction temperature and the HCl/CH_4 ratio in the feed.

3.5. Stability of EuOCl. Finally, EuOCl was tested for its stability under oxychlorination conditions at 450 °C. Over a period of 48 h, the catalyst was exposed to increasing HCl concentrations with constant CH_4 and O_2 concentration and total flow. The X_{CH_4} product yields and reaction selectivity are plotted in Figure 11A. At the start, a drop in X_{CH_4} and yields of CH_3Cl and CO are visible. This effect is most probably caused by the decrease in the surface area of the catalyst because no prechlorination step was performed.[22] After 2 h of reaction, the CH_3Cl yield stabilizes, while the CO yield gradually decreases. This is also visible from the selectivity plot shown in Figure 11A where S_{CO} decreases from 44 to 37%, while S_{CH_3Cl} increases with the same percentage and $S_{CH_2Cl_2}$ remains the same. Subsequently, the HCl concentration was increased to 20% without increasing the total flow. An immediate jump in CH_3Cl (+2.2%), CH_2Cl_2 (+0.6%), and CO (+0.8%) yield occurs due to the increased chlorination rate of the catalyst surface. However, now, the CH_3Cl yield drops over time (−0.8%), while the CO yield remains constant.

https://doi.org/10.1021/acscatal.1c00393
ACS Catal. 2021, 11, 10574−10588

Again, a jump in yield is observed when increasing the HCl concentration to 40% for CH_3Cl (+2%), CH_2Cl_2 (+1.1%), and CO (+1%). The selectivity of all the products remains fairly constant over the duration of 10 h. The yields of the reaction products decrease slightly. Up to this point, the catalyst material behaves in the same fashion. However, when the HCl concentration is further increased from 40 to 60%, a different catalytic behavior is observed.

Right from the moment that the HCl concentration was further increased, the CO yield drops gradually (−1.1%), while the CM yields do not show any downward trend. S_{CO} is reduced from 26 to 20%, a relative decrease of 23%. Under these conditions, we observe a low $CHCl_3$ yield of 0.4%, which correlates to a S_{CHCl_3} of 2.4%. Near the end, the production of CH_3Cl increases slightly after which it starts to drop when the HCl concentration is further increased to 80%.

Just before the feed ratio is adjusted to 80% HCl, we observe a change of the catalyst property, as analyzed with *operando* Raman spectroscopy. The *operando* Raman spectra in the spectral range of 180−500 cm^{-1} are plotted *versus* the time on stream in Figure 11B. Furthermore, some individual *operando* Raman spectra are plotted of moments before and after changing the feed ratio to 80% HCl in Figure 11C. After 38 h time on stream, the Raman spectra start to change and the overall intensity decreases, which are indicative of the transition from EuOCl to $EuCl_3$.

The full chlorination of the catalyst material has severe effects on the catalytic behavior. While the selectivity of the reaction does not seem to be affected by the changing catalyst properties, the catalyst deactivates. The decreasing CO yield trend is continued, but the CH_3Cl yield is negatively affected over time. From previous experiments, we proved that EuOCl was difficult to chlorinate, especially under oxychlorination conditions. We now show that bulk transformation of EuOCl to $EuCl_3$ occurs under very high HCl concentrations (≥60%) over prolonged reaction times. Moreover, bulk chlorination is unwanted because a decrease in the product yield was observed. A balanced HCl concentration in the feed mixture is therefore crucial to enhance the surface chlorination rate but also to prevent bulk chlorination. An HCl concentration between 40 and 60% appears to be optimal, in terms of catalyst stability and catalytic performance.

4. CONCLUSIONS

We have investigated a series of lanthanide oxide chlorides (*i.e.*, LnOCl with Ln = La, Pr, Nd, Sm, Eu, Gd, Tb, Dy, or Ho) and Er- and Yb-based catalyst materials, which turned to be all active in the catalytic oxychlorination of CH_4. Based on their catalytic activity, the following ranking can be made as follows: Eu > Tb > Gd ∼ Ho ∼ Er > Dy > Sm > Pr ≈ Nd ≈ La ≈ Yb. Furthermore, from all the catalyst materials under investigation, EuOCl exhibited the highest activity and the best selectivity toward CH_3Cl. The catalytic performance of EuOCl could be further increased by altering the HCl concentration, as an excess of HCl doubled the activity and lowered the CO selectivity. Exceptionally high conversion levels (∼40%) could be reached, while maintaining a low CO_x selectivity (<15%). *Operando* Raman spectroscopy revealed that the surface chlorination of the catalyst surface is rate-limiting, and hence, the activity of both the MOC and the HCl oxidation is boosted when an excess HCl is present. *Operando* photoluminescence spectroscopy of Eu^{3+} revealed that the bulk of EuOCl was subjected to major changes, and the state of the catalyst is determined by the CH_4/HCl ratio. However, if high HCl concentrations are applied at low X_{CH_4} over prolonged reaction times, EuOCl does chlorinate fully and the catalyst activity is lowered. The tunable activity and selectivity by altering the HCl concentration in the feed and the reaction make EuOCl a very interesting candidate as a catalytic material for a viable CH_4 oxychlorination process.

■ ASSOCIATED CONTENT

Supporting Information

The Supporting Information is available free of charge at https://pubs.acs.org/doi/10.1021/acscatal.1c00393.

Details of the reactor setup and additional characterization (N_2 physisorption and TEM), activity (GC), and spectroscopy (Raman, photoluminescence) (PDF)

■ AUTHOR INFORMATION

Corresponding Author

Bert M. Weckhuysen − *Inorganic Chemistry and Catalysis Group, Debye Institute for Nanomaterials Science, Utrecht University, 3584 CG Utrecht, The Netherlands;* orcid.org/0000-0001-5245-1426; Email: B.M.Weckhuysen@uu.nl

Authors

Bas Terlingen − *Inorganic Chemistry and Catalysis Group, Debye Institute for Nanomaterials Science, Utrecht University, 3584 CG Utrecht, The Netherlands;* orcid.org/0000-0001-8973-6601

Ramon Oord − *Inorganic Chemistry and Catalysis Group, Debye Institute for Nanomaterials Science, Utrecht University, 3584 CG Utrecht, The Netherlands*

Mathieu Ahr − *Nobian, 7418 AJ Deventer, The Netherlands*

Eline Hutter − *Inorganic Chemistry and Catalysis Group, Debye Institute for Nanomaterials Science, Utrecht University, 3584 CG Utrecht, The Netherlands;* orcid.org/0000-0002-5537-6545

Coert van Lare − *Nobian, 7418 AJ Deventer, The Netherlands*

Complete contact information is available at: https://pubs.acs.org/10.1021/acscatal.1c00393

Author Contributions

The manuscript was written through contributions of all authors. All authors have given approval to the final version of the manuscript.

Funding

The authors thank ARC CBBC for research funding.

Notes

The authors declare no competing financial interest.

■ ACKNOWLEDGMENTS

This work is part of the Advanced Research Center for Chemical Building Blocks (ARC CBBC), which is co-founded and co-financed by the Netherlands Organisation for Scientific Research (NWO) and the Netherlands Ministry of Economic Affairs and Climate Policy. Furthermore, the authors would like to thank Matteo Monai for helping with finalizing the manuscript.

■ REFERENCES

(1) *BP Energy Outlook*, 2019.report

(2) Wang, B.; Albarracín-Suazo, S.; Pagán-Torres, Y.; Nikolla, E. Advances in Methane Conversion Processes. *Catal. Today* **2017**, *285*, 147−158.
(3) Jiao, F.; Li, J.; Pan, X.; Xiao, J.; Li, H.; Ma, H.; Wei, M.; Pan, Y.; Zhou, Z.; Li, M.; Miao, S.; Li, J.; Zhu, Y.; Xiao, D.; He, T.; Yang, J.; Qi, F.; Fu, Q.; Bao, X. Selective Conversion of Syngas to Light Olefins. *Science* **2016**, *351*, 1065−1068.
(4) Alvarez-Galvan, M. C.; Mota, N.; Ojeda, M.; Rojas, S.; Navarro, R. M.; Fierro, J. L. G. Direct Methane Conversion Routes to Chemicals and Fuels. *Catal. Today* **2011**, *171*, 15−23.
(5) Taifan, W.; Baltrusaitis, J. CH_4 Conversion to Value Added Products: Potential, Limitations and Extensions of a Single Step Heterogeneous Catalysis. *Appl. Catal., B* **2016**, *198*, 525−547.
(6) Zichittella, G.; Aellen, N.; Paunović, V.; Amrute, A. P.; Pérez-Ramírez, J. Olefins from Natural Gas by Oxychlorination. *Angew. Chem., Int. Ed.* **2017**, *56*, 13670−13674.
(7) Kim, J.; Ryou, Y.; Hwang, G.; Bang, J.; Jung, J.; Bang, Y.; Kim, D. H. Oxychlorination of Methane over FeOx/CeO2 Catalysts. *Korean J. Chem. Eng.* **2018**, *35*, 2185−2190.
(8) Paunović, V.; Zichittella, G.; Hemberger, P.; Bodi, A.; Pérez-Ramírez, J. Selective Methane Functionalization via Oxyhalogenation over Supported Noble Metal Nanoparticles. *ACS Catal.* **2019**, *9*, 1710−1725.
(9) He, J.; Xu, T.; Wang, Z.; Zhang, Q.; Deng, W.; Wang, Y. Transformation of Methane to Propylene: A Two-Step Reaction Route Catalyzed by Modified CeO_2 Nanocrystals and Zeolites. *Angew. Chem., Int. Ed.* **2012**, *51*, 2438−2442.
(10) Peringer, E.; Podkolzin, S. G.; Jones, M. E.; Olindo, R.; Lercher, J. A. $LaCl_3$-Based Catalysts for Oxidative Chlorination of CH_4. *Top. Catal.* **2006**, *38*, 211−220.
(11) Peringer, E.; Salzinger, M.; Hutt, M.; Lemonidou, A. A.; Lercher, J. A. Modified Lanthanum Catalysts for Oxidative Chlorination of Methane. *Top. Catal.* **2009**, *52*, 1220−1231.
(12) Paunović, V.; Zichittella, G.; Moser, M.; Amrute, A. P.; Pérez-Ramírez, J. Catalyst Design for Natural-Gas Upgrading through Oxybromination Chemistry. *Nat. Chem.* **2016**, *8*, 803−809.
(13) Paunović, V.; Lin, R.; Scharfe, M.; Amrute, A. P.; Mitchell, S.; Hauert, R.; Pérez-Ramírez, J. Europium Oxybromide Catalysts for Efficient Bromine Looping in Natural Gas Valorization. *Angew. Chem., Int. Ed.* **2017**, *56*, 9791−9795.
(14) Zichittella, G.; Paunović, V.; Amrute, A. P.; Pérez-Ramírez, J. Catalytic Oxychlorination versus Oxybromination for Methane Functionalization. *ACS Catal.* **2017**, *7*, 1805−1817.
(15) Paunović, V.; Artusi, M.; Verel, R.; Krumeich, F.; Hauert, R.; Pérez-Ramírez, J. Lanthanum Vanadate Catalysts for Selective and Stable Methane Oxybromination. *J. Catal.* **2018**, *363*, 69−80.
(16) Lin, R.; Amrute, A. P.; Pérez-Ramírez, J. Halogen-Mediated Conversion of Hydrocarbons to Commodities. *Chem. Rev.* **2017**, *117*, 4182−4247.
(17) Van Der Heijden, A. W. A. M.; Bellière, V.; Alonso, L. E.; Daturi, M.; Manoilova, O. V.; Weckhuysen, B. M. Destructive Adsorption of CCl_4 over Lanthanum-Based Solids: Linking Activity to Acid-Base Properties. *J. Phys. Chem. B* **2005**, *109*, 23993−24001.
(18) Schweizer, A. E.; Jones, M. E.; Hickman, D. A. Oxidative Halogenation of C1 Hydrocarbons to Halogenated C1 Hydrocarbons and Integrated Processes Related Thereto. U.S. Patent 6,452,058 B1, 2002.
(19) Scharfe, M.; Zichittella, G.; Paunović, V.; Pérez-Ramírez, J. Ceria in Halogen Chemistry. *Chin. J. Catal.* **2020**, *41*, 915−927.
(20) Sabnis, K. D.; Fickel, D. W.; Shou, H.; Casper, M. D.; Kulkarni, N.; Araujo, A.; Mamedov, E. Selective Monochlorination of Methane via Elimination of Dichloromethane from the Oxychlorination Product Stream. *React. Kinet. Mech. Catal.* **2019**, *127*, 413−423.
(21) Podkolzin, S. G.; Stangland, E. E.; Jones, M. E.; Peringer, E.; Lercher, J. A. Methyl Chloride Production from Methane over Lanthanum-Based Catalysts. *J. Am. Chem. Soc.* **2007**, *129*, 2569−2576.
(22) Peringer, E.; Tejuja, C.; Salzinger, M.; Lemonidou, A. A.; Lercher, J. A. On the Synthesis of $LaCl_3$ Catalysts for Oxidative Chlorination of Methane. *Appl. Catal., A* **2008**, *350*, 178−185.
(23) Stauffer, J. E. Methane to Olefins. U.S. Patent 7,091,391 B2, 2006.
(24) Clarke, W. D.; Haymon, T. D.; Henley, J. P.; Hickman, D. A.; Jones, M. E.; Miller, M. C.; Morris, T. E.; Reed, D. J.; Samson, L. J.; Schweizer, A. E.; Smith, S. A. Production of Vinyl Halide from Single Carbon Feedstocks. U.S. Patent 20,050,027,084 A1, 2005.
(25) Gulotty, R. J.; Jones, M. E.; Hickman, D. A. Oxyhalogenation Process Using Catalyst Having Porous Rare Earth Halide Support. U.S. Patent 6,680,415 B1, 2004.
(26) Nubel, P. O.; Satek, L. C.; Spangler, M. J.; Lutman, C. A.; Michaels, G. O. Halogen-Assisted Conversion of Lower Alkanes. U.S. Patent 5,087,786 A, 1991.
(27) Podkolzin, S. G.; Stangland, E. E.; Schweizer, A. E.; Jones, M. E. Oxidative Halogenation of C_1 Hydrocarbons to Halogenated C_1 Hydrocarbons. U.S. Patent 20,080,275,279 A1, 2008.
(28) Bowman, R. G.; Stangland, E. E.; Jones, M. E.; Millar, D. M.; Podkolzin, S. G.; Stears, B. A.; Wehmeyer, R. M. Oxidative Mono-Halogenation of Methane. U.S. Patent 8,674,149 B2, 2014.
(29) Saadun, A. J.; Zichittella, G.; Paunović, V.; Markaide-Aiastui, B. A.; Mitchell, S.; Pérez-Ramírez, J. Epitaxially Directed Iridium Nanostructures on Titanium Dioxide for the Selective Hydrodechlorination of Dichloromethane. *ACS Catal.* **2020**, *10*, 528−542.
(30) Olah, G. A.; Gupta, B.; Felberg, J. D.; Ip, W. M.; Husain, A.; Karpeles, R.; Lammertsma, K.; Melhotra, A. K.; Trivedi, N. J. Electrophilic reactions at single bonds. 20. Selective monohalogenation of methane over supported acidic or platinum metal catalysts and hydrolysis of methyl halides over .gamma.-alumina-supported metal oxide/hydroxide catalysts. A feasible path for the oxidative conversion of methane into methyl alcohol/dimethyl ether. *J. Am. Chem. Soc.* **1985**, *107*, 7097−7105.
(31) van der Heijden, A. W. A. M.; Podkolzin, S. G.; Jones, M. E.; Bitter, J. H.; Weckhuysen, B. M. Catalytic Hydrogen-Chlorine Exchange between Chlorinated Hydrocarbons under Oxygen-Free Conditions. *Angew. Chem., Int. Ed.* **2008**, *47*, 5002−5004.
(32) Treger, Y. A.; Rozanov, V. N.; Sokolova, S. V.; Murashova, O. P. Producing Ethylene and Propylene from Natural Gas via the Intermediate Synthesis of Methyl Chloride and Its Subsequent Catalytic Pyrolysis. *Catal. Ind.* **2012**, *4*, 231−235.
(33) Van der Avert, P.; Weckhuysen, B. M. Low-Temperature Catalytic Destruction of CCl_4, $CHCl_3$ and CH_2Cl_2 over Basic Oxides. *Phys. Chem. Chem. Phys.* **2004**, *6*, 5256.
(34) Pyykkö, P. Relativistic Effects in Structural Chemistry. *Chem. Rev.* **1988**, *88*, 563−594.
(35) Garcia, E.; Corbett, J. D.; Ford, J. E.; Vary, W. J. Low-Temperature Routes to New Structures for Yttrium, Holmium, Erbium, and Thulium Oxychlorides. *Inorg. Chem.* **1985**, *24*, 494−498.
(36) van der Heijden, A. W. A. M.; Garcia Ramos, M.; Weckhuysen, B. M. Intermediates in the Destruction of Chlorinated C_1 Hydrocarbons on La-Based Materials: Mechanistic Implications. *Chem.—Eur. J.* **2007**, *13*, 9561−9571.
(37) van der Heijden, A. W. A. M.; Mens, A. J. M.; Bogerd, R.; Weckhuysen, B. M. Dehydrochlorination of Intermediates in the Production of Vinyl Chloride over Lanthanum Oxide-Based Catalysts. *Catal. Lett.* **2008**, *122*, 238−246.
(38) Van der Avert, P.; Podkolzin, S. G.; Manoilova, O.; de Winne, H.; Weckhuysen, B. M. Low-Temperature Destruction of Carbon Tetrachloride over Lanthanide Oxide-Based Catalysts: From Destructive Adsorption to a Catalytic Reaction Cycle. *Chem.—Eur. J.* **2004**, *10*, 1637−1646.
(39) Zichittella, G.; Polyhach, Y.; Tschaggelar, R.; Jeschke, G.; Pérez-Ramírez, J. Quantification of Redox Sites during Catalytic Propane Oxychlorination by Operando EPR Spectroscopy. *Angew. Chem., Int. Ed.* **2021**, *60*, 3596−3602.
(40) Haeuseler, H. Raman Spectra of Single Crystals of LaOCl. *J. Raman Spectrosc.* **1984**, *15*, 120−121.
(41) Weckhuysen, B. M.; Rosynek, M. P.; Lunsford, J. H. Destructive Adsorption of Carbon Tetrachloride on Lanthanum and Cerium Oxides. *Phys. Chem. Chem. Phys.* **1999**, *1*, 3157−3162.

https://doi.org/10.1021/acscatal.1c00393
ACS Catal. 2021, 11, 10574−10588

(42) Kim, D.; Jeong, J. R.; Jang, Y.; Bae, J.-S.; Chung, I.; Liang, R.; Seo, D.-K.; Kim, S.-J.; Park, J.-C. Self-Emitting Blue and Red EuOX (X = F, Cl, Br, I) Materials: Band Structure, Charge Transfer Energy, and Emission Energy. *Phys. Chem. Chem. Phys.* **2019**, *21*, 1737−1749.
(43) She, C. Y.; Broberg, T. W.; Edwards, D. F. Raman Spectra of Tetragonal Lanthanide Oxychlorides Obtained from Polycrystalline and Single-Crystal Samples. *Phys. Rev. B: Solid State* **1971**, *4*, 1580−1583.
(44) Zakir'yanova, I. D.; Salyulev, A. B.; Khokhlov, V. A. Raman Spectroscopy Study of the Phase Transitions in Rare-Earth Metal Trichlorides. *Russ. Metall.* **2011**, *2011*, 754−759.
(45) McBee, E. T.; Hass, H. B.; Neher, C. M.; Strickland, H. Chlorination of Methane. *Ind. Eng. Chem.* **1942**, *34*, 296−300.
(46) Milligan, B.; Dumesic, J. A. Physical, Adsorptive, and Catalytic Properties of Platinum Supported on Silica Modified with Europium Oxide. *J. Catal.* **1989**, *115*, 180−193.
(47) Van der Avert, P.; Weckhuysen, B. M. Low-Temperature Destruction of Chlorinated Hydrocarbons over Lanthanide Oxide Based Catalysts. *Angew. Chem., Int. Ed.* **2002**, *41*, 4730−4732.
(48) Rioux, R. M.; Song, H.; Hoefelmeyer, J. D.; Yang, P.; Somorjai, G. A. High-Surface-Area Catalyst Design: Synthesis, Characterization, and Reaction Studies of Platinum Nanoparticles in Mesoporous SBA-15 Silica. *J. Phys. Chem. B* **2005**, *109*, 2192−2202.
(49) Vogt, C.; Groeneveld, E.; Kamsma, G.; Nachtegaal, M.; Lu, L.; Kiely, C. J.; Berben, P. H.; Meirer, F.; Weckhuysen, B. M. Unravelling Structure Sensitivity in CO_2 Hydrogenation over Nickel. *Nat. Catal.* **2018**, *1*, 127−134.
(50) Hölsä, J.; Porcher, P. Free Ion and Crystal Field Parameters for REOCl:Eu^{3+}. *J. Chem. Phys.* **1981**, *75*, 2108−2117.
(51) Rabouw, F. T.; Prins, P. T.; Norris, D. J. Europium-Doped $NaYF_4$ Nanocrystals as Probes for the Electric and Magnetic Local Density of Optical States throughout the Visible Spectral Range. *Nano Lett.* **2016**, *16*, 7254−7260.
(52) Lui, R.; Yan, Q.; Zhai, Y.; QI, H.; Hsia, Y.; Jiang, J.; Gonser, U. Investigation of the Solid-Solid Surface Adsorption of Eu_2O_3 on Amorphous Al_2O_3. *Hyperfine Interact.* **1992**, *69*, 847−850.
(53) Quesada, A.; Del Campo, A.; Fernández, J. F. Stabilization of Cubic Phase in Dense Eu_2O_3 Ceramics. *Mater. Lett.* **2015**, *157*, 77−80.

https://doi.org/10.1021/acscatal.1c00393
ACS Catal. 2021, 11, 10574−10588